Cancer Biol Med 2016. doi: 10.20892/j.issn.2095-3941.2016.0052

REVIEW

OPEN ACCESS

Advances in biodegradable nanomaterials for photothermal therapy of cancer

Chao-Feng He[1,2], Shun-Hao Wang[2], Ying-Jie Yu[3], He-Yun Shen[2], Yan Zhao[4], Hui-Ling Gao[2], Hai Wang[5], Lin-Lin Li[6], Hui-Yu Liu[2]

[1]School of Material Science and Engineering, Henan Polytechnic University, Jiaozuo 454000, China; [2]Beijing Key Laboratory of Bioprocess, Beijing University of Chemical Technology, Beijing 100029, China; [3]Department of Materials Science and Engineering, State University of New York at Stony Brook, Stony Brook, NY 11790, USA; [4]Department of Emergency, Shandong Heze Municipal Hospital, Heze 274031, China; [5]CAS Key Laboratory for Biomedical Effects of Nanomaterials & Nanosafety, CAS Center for Excellence in Nanoscience, National Center for Nanoscience and Technology (NCNST), Beijing 100190, China; [6]Beijing Institute of Nanoenergy and Nanosystems, National Center for Nanoscience and Technology (NCNST), Chinese Academy of Sciences, Beijing 100083, China

ABSTRACT Photothermal cancer therapy is an alternative to chemotherapy, radiotherapy, and surgery. With the development of nanophotothermal agents, this therapy holds immense potential in clinical translation. However, the toxicity issues derived from the fact that nanomaterials are trapped and retained in the reticuloendothelial systems limit their biomedical application. Developing biodegradable photothermal agents is the most practical route to address these concerns. In addition to the physicochemical properties of nanomaterials, various internal and external stimuli play key roles on nanomaterials uptake, transport, and clearance. In this review, we summarized novel nanoplatforms for photothermal therapy; these nanoplatforms can elicit stimuli-triggered degradation. We focused on the recent innovative designs endowed with biodegradable photothermal agents under different stimuli, including enzyme, pH, and near-infrared (NIR) laser.

KEYWORDS Photothermal therapy; enzyme stimuli; pH stimuli; near-infrared laser stimuli; biodegradability

Introduction

Photothermal therapy (PTT), which employs photothermal agents (PTAs) to convert light to heat for the thermal ablation of cancer cells, has attracted great attention because of certain advantages, such as minimal invasiveness, high specificity, few complications, and low toxicity to normal tissues[1]. Studies have been devoted in the exploration of numerous nano-PTAs for PTT, including gold-based nanostructures[2-4], conjugated polymers[5,6], carbon nanomaterials (NMs)[7,8], semiconductor NMs[9,10], and other currently developed nano-PTAs[11,12]. Although most of them exhibit high therapeutic efficacy, clinical translation has been restricted because of certain concerns with regard to their long-term accumulation in the main organs, which could result in toxicity[13], side effects[14], and inflammatory response[15]. Our recent study evaluated the biodistribution and clearance of gold nanoshells during which polyethylene glycol (PEG)-functionalized gold nanoshells were mostly retained in the liver and spleen, even at 15 days after injection[16]. The slow clearance from these organs was consistent with the low excretion of Au content from urine and feces samples[17]. According to the US Food and Drug Administration (FDA), theranostic agents in clinics must be eliminated or cleared in a reasonable period of time[18]. Therefore, biodegradability and biocompatibility have become essential requirements for the clinical applications of PTAs.

Novel nanoplatforms that can elicit stimuli-responsive degradation show great promise in nanoscience and nanomedicine. Biodegradable polymers are preferable because of their good biocompatibility, identified degradation mechanism, and set of metabolic pathways. Conventional methods for the preparation of stimuli-responsive polymers involve the incorporation of cleavable linkages into the main chains[19] or pendant chains[20]. Their

Correspondence to: Hui-Yu Liu
E-mail: liuhy@mail.buct.edu.cn
Received July 20, 2016; accepted August 30, 2016.
Available at www.cancerbiomed.org

long molecular chains are first ruptured by biological activity[21]. Then the fragmented carbon chains are metabolized by different organisms. In contrast to the organic NMs, inorganic nanoparticles have limited clinical translations because of the concerns regarding their long-term toxicity. A recent review introduced certain biodegradable inorganic materials investigated in preclinical studies[22]. Iron oxide nanoparticles (IONPs) have been found to release a trace element of Fe ions to the bloodstream during certain metabolic processes[23]. Porous silicon nanoparticles are degraded into water-soluble silicic acid and then are eliminated from the body in 1 week[24]. As NMs smaller than 5.5 nm can achieve renal clearance[25], inorganic NMs with smaller sizes are likely degraded into nontoxic products and eliminated through the kidneys[24].

In view of the expanding research on PTAs, the most recent and relevant reviews have focused on the synthesis and applications of PTAs[26]. However, the processes in the biodegradation of PTAs require further research. In this review, we focused on the different types of stimuli, including those in the internal environment (enzymes, pH, and temperature) and in the external environment (light irradiation, magnetic field, and ultrasound), which are exploited to initiate the degradation of PTAs. Along with the innovative design or structure that can be subjected to biodegradation under these stimuli, the photothermal efficiency and degradation behavior were addressed. The major targeting delivery and clearance pathway of the biodegradable PTAs were discussed. Finally, we recapitulated these biodegradable PTAs and the challenges in PTT with regard to clinical application of the former.

Stimuli-responsive degradation

Stimuli-responsive degradation of PTAs can decrease the accumulation and retention of PTAs *in vivo* through effective clearance. They undergo hydrolytic cleavage, surface oxidation, or structural fracture in response to a certain stimulus. In this section, we discuss certain of biodegradable PTAs that take advantage of various stimuli, such as enzyme, pH, and near-infrared (NIR) laser.

Enzyme-induced degradation

Enzyme-catalyzed hydrolysis degradation

Phospholipase A2 (PLA2) is a well-known hydrolysis agent used for recognizing and hydrolyzing the *sn*-2 acyl bond of phospholipids that releases free fatty acids and lysophosphatidic acid[27]. These enzymes are commonly found in mammalian tissues and are overexpressed in tumors. This unique characteristic of PLA2 can enable the use of biodegradable lipid-based structures in biomedical applications. For example, liposomes with lipid bilayers have been approved as drug carriers because of their biodegradability[28]. In this regard,many efforts have been made to improve their NIR absorption. Several methods to improve their NIR absorption were thus discovered, such as the loading of indocyanine green (ICG) in aqueous core[29] or lipid bilayer of liposome[30].

In 2011, Lovell et al.[31] developed a novel liposome-like structure (porphysomes) by self-assembled porphyrin analogue-lipid conjugation (1:1 molecule ratio). The porphyrin analogue (pyropheophorbide or bacteriochlorophyll) was located at the *sn*-2 position of the lysophosphatidylcholine (**Figure 1A**). Alternatively, metal ions can be inserted into the porphyrin-lipid structure to form unique metal-chelating bilayers. These liposome-like porphysomes containing approximately 80,000 porphyrins can effectively convert light into heat through the fluorescence-quenching porphyrins in the intact porphysomes. This high conversion efficiency is comparable with gold nanorods under 673 nm laser irradiation (**Figure 1B**). When exposed to laser (658 nm, 1.9 W/cm^2), the injected pyropheophorbide-porphysomes (42 mg/kg) can lead to a temperature increase (up to 60 °C), which can completely eradicate KB tumors in xenograft-bearing mice (**Figure 1C**). Jin et al.[32] corroborated the toxicity of the photothermal effect in tumors but not the photodynamic effect. They also found that the heat generated by the porphysomes is highly dependent on their integrated structure, and the singlet oxygen production can restore on the disrupting structure. For biodegradability, pyropheophorbide-porphysomes could degrade into the starting material when incubated with lipase, as shown in **Figure 1A**. The nature of the enzymatic biodegradation *in vitro* was likely because of the cleaving of the porphyrin by lipase in the *sn*-2 position of lipid[33]. Lovell et al.[33] further confirmed the substantial degradation of pyropheophorbide-porphysomes after *in vivo* intravenous (IV) administration. Moreover, no toxicity was observed after the introduction of pyropheophorbide-porphysomes (1,000 mg/kg) in the system, thus it is highly biocompatible.

Liposome-gold clusters are another lipid-based structures formed through the assembling of gold clusters on the liposome core[34]. The high-density packing of gold clusters retains the NIR absorption property of the metallic shells, and the liposome scaffold provides degradability. According

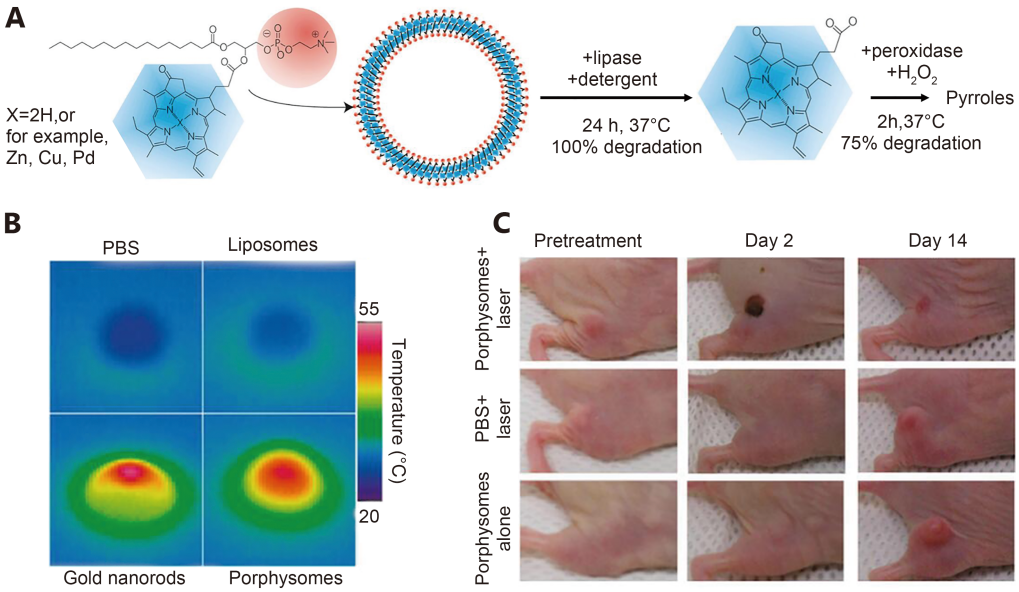

Figure 1 (A) Illustration of formation and enzymatic degradation process of a pyropheophorbide-lipid porphysomes. Porphysome were assembled from the phospholipid (red) conjugated with porphyrin (blue), and degraded by incubation with detergent and lipase. (B) Photothermal images of solutions (PBS, liposome, gold nanorods, porphysomes) after 673 nm laser light irradiation. (C) Photographs of KB tumor-bearing mice after photothermal therapy using porphysomes. Reproduced with permission from Ref. 31. Copyright 2009 Nature Publishing Group.

to the literature, the destabilization of the liposome template facilitates the splitting of gold nanoparticles into small particles with a renal clearance size (5–6 nm) (**Figure 2A**). When the liposome-gold clusters suspension was incubated with PLA2 and Ca^{2+} at 45 °C overnight, the plasmon resonance gradually disappeared and changed its color. As for the Triton X-100, the remaining suspension showed an average diameter of ~5.7 nm, indicating the degradation of the composite. Troutman et al.[34] first reported the architecture of the liposome-gold clusters based on a dialkyl phosphatidylcholine (DPPC) template. Rengan et al.[35] investigated the antitumor effects of liposome-gold clusters on MCF-7 cancer cell and performed a pharmacokinetic study on liposome-gold clusters using mice. For PTT, 15 μg/mL liposome-gold clusters can efficiently ablate cancer cells, which is indicated by the breaking of the DNA double strands under NIR laser (750 nm, 650 mW) illumination for 4 min (**Figure 2B**). Quantitative analysis on feces and urine samples identified the hepato-biliary and renal pathway clearance of the small particles (**Figure 2C**). Liposome-gold clusters tend to aggregate in the major organs and they gradually cleave into smaller particles after IV injection (**Figure 2D**). Apart from the enzymatic degradation, the NIR light can be used to initiate the destabilization of the liposome-gold clusters for spatial- and temporal-controlled content release[36-38].

Enzyme-catalyzed oxidation degradation

Horseradish peroxidase (HRP) is among the extensively used metalloenzymes for catalytic oxidation in a variety of substrates, frequently in the presence of hydrogen peroxide (H_2O_2). This oxidation action is known to imitate the redox process in a cellular metabolism. In 2008, researchers discovered that single-walled carbon nanotubes (SWNTs) can be degraded by HRP in the presence of H_2O_2. After 12 weeks of incubation in phosphate buffered saline (PBS) at 4 °C, no distinct tubular structure of carbon nanotubes were observed, thereby indicating that nearly all nanotube materials were degraded[39]. To further investigate the mechanism of HRP-catalyzed degradation, Allen et al.[40] compared the degradation course of the carboxylated SWNTs and the pristine SWNTs using HRP and H_2O_2. Their data suggested that the hydrophobic surface on pristine SWNTs were resistant to the HRP catalyst, whereas the carboxylated sites on the SWNTs facilitated the adsorption of HRP, thereby enhancing the catalytic effect. Moreover, the degraded products gradually evolved from oxidized aromatic fragments to CO_2. These results can be extended to the

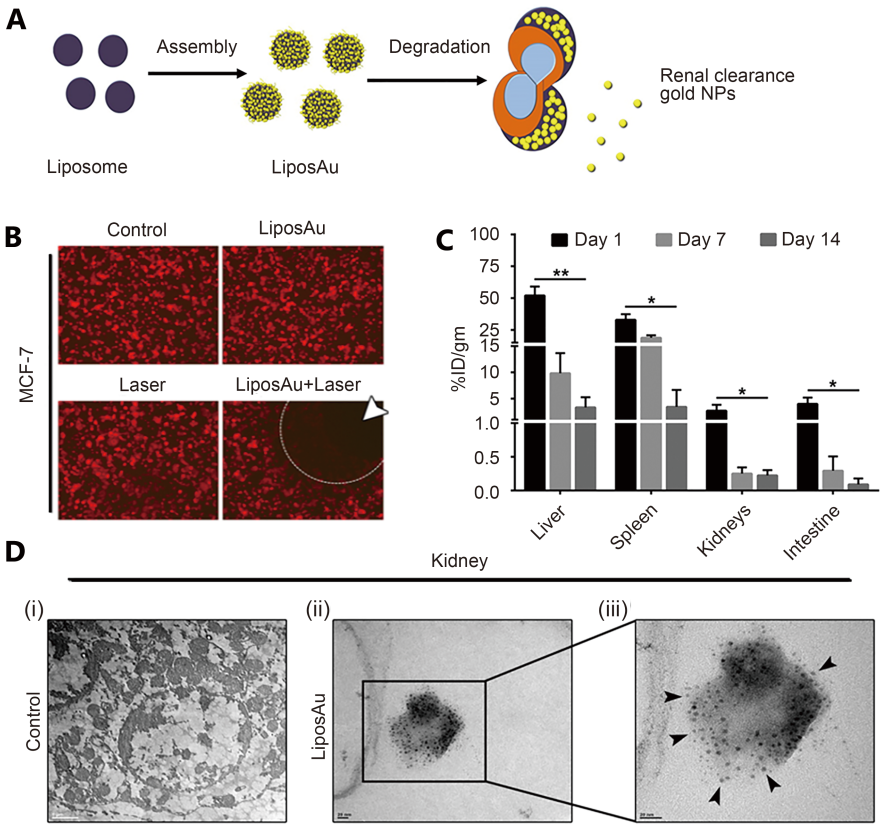

Figure 2 (A) Illustration of the formation and degradation processes of liposome-gold clusters (LiposAu). (B) Fluorescence micrograph images of MCF-7 cancer cell after photothermal effect (750 nm, 2.3 w/cm^2, 4 min) induced by liposome-gold clusters (15 μg/mL). Red color represents TurboFP fluorescent protein overexpressed in cancer cells. (C) Tissue biodistribution of Au *in vivo* at different days after IV injection of liposome-gold clusters. (D) TEM of kidney tissue without any treatment (i), and with liposome-gold clusters NP (ii). Liposome-gold clusters are cleaved into small gold nanoparticles less than 5 nm (iii). Reproduced with permission from Ref. 35. Copyright 2015 American Chemical Society.

degradation of SWNTs in living systems[41-44]. When incubated with neutrophils and macrophages, the SWNTs were also degraded by myeloperoxidase. Particularly, the SWNTs first produced defects in the outer wall, and the developed defects initiated structure alterations over increased incubation time[41]. Moreover, the experiments on mice proved *in vivo* that the oxidative biodegradation of SWNTs is associated to human myeloperoxidase[42]. Some researchers also reported that SWNTs can be degraded in the brain cortex[45] and in the primary microglial culture models[46]. They emphasized that the defects or the functionalized sites on carbon nanotubes significantly facilitate enzymatic action. HRP-induced degradation of multiwalled carbon nanotubes with defective sites in the graphitic walls was demonstrated by Zhao et al.[47]. Carbon nanotubes cancer mediate photothermal tumor destruction which has been documented in several studies[48-53], but their slow degradation rate *in vivo* and their degradation byproduct such as reactive oxygen species[43,44] are still unsuitable for clinical application. The structural design and surface functionalization that exposed more active sites (carboxylic groups, defects) on the graphitic surface could accelerate this enzymatic degradation.

Graphene oxide (GO) is another graphite derivative that have shown great potential for biological applications in photothermal therapy and drug delivery. The development of biodegradable GOs is of great importance, and can promote the development of nanomedicine. As GOs have similar sp^2 allotropes of carbon similar to carbon nanotubes, they were also reported to be able to undergo similar HRP-induced oxidative degradation in the presence of H_2O_2[54]. **Figure 3A** shows the molecular modeling of an HRP on a GO. Because

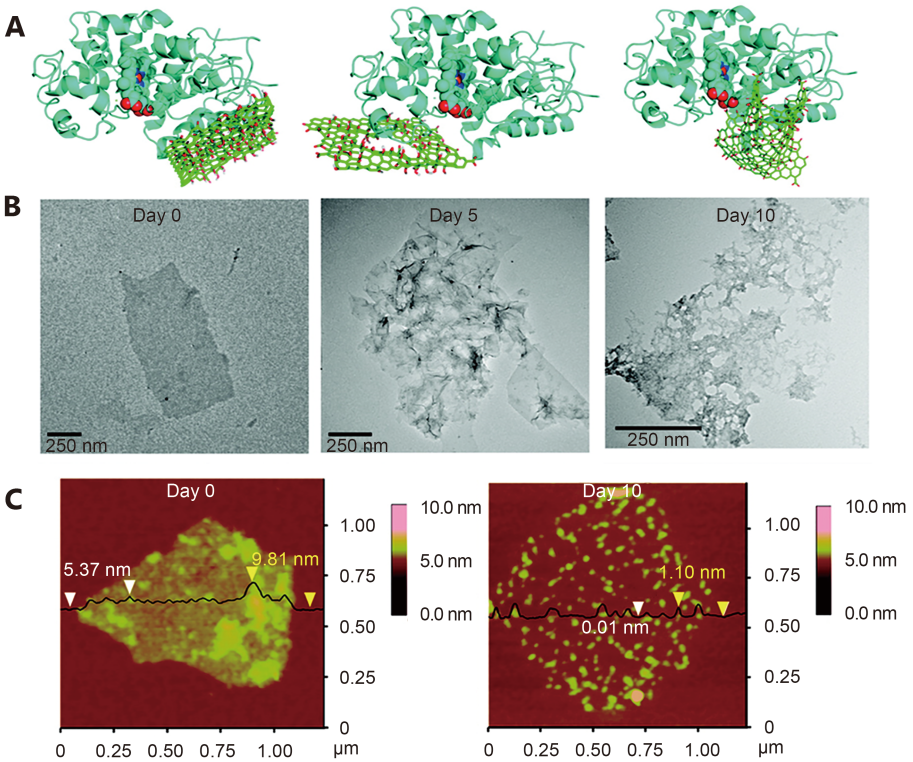

Figure 3 (A) Illustration of the binding position of HRP on graphene oxide, holey graphene oxide, and a small sheet of graphene oxide (from left to right). (B) TEM image of graphene oxide incubated with solution containing HRP and 40 μM H_2O_2 after 0, 5, 10 days. (C) Atomic force microscopy (AFM) images of graphene oxide incubated with HRP after 0 day and 10 days. The sheet heights of the graphene oxide in day 0 and day 10 are 9.81 nm and 1.10 nm, respectively. Reproduced with permission from Ref. 54. Copyright 2011 American Chemical Society.

of the effect of the HRP, the basal plane of the GO gradually produced certain holes, which can act as cleavage sites for carbon-carbon bonds. This result is consistent with the observations in the transmission electron microscopy (TEM) images (**Figure 3B**) and atomic force microscopy (AFM) images (**Figure 3C**). Afterward,a gradual tendency of graphene to disorganize its structure *in vivo* was observed at the 3rd month after injection. This process was related to the processes of the tissue-bound macrophages. However, the problems of long-term retention still cannot be addressed, which lead to toxicity risks and immune response[55]. To improve its biocompatibility, GO is usually functionalized with PEG or bovine serum albumin (BSA), producing PEG-GO and BSA-GO. However, PEG-GO and BSA-GO cannot degrade in HRP and H_2O_2 because the PEG or BSA in the GO surface inhibits the interaction between the HRP and GO[56]. When GO was functionalized with a cleavable PEG (mPEG-SS-NH_2), the generated GO-SS-PEG cleaved the disulfide linkages by dithiothreitol, resulting in the degradation in HRP and H_2O_2[56]. Similarly, the GO-SS-PEG degradation in A549 cells can be triggered by a high concentration of glutathione[57].

pH-induced degradation

The interstitial pH of tumor tissues is ~6.8, which is lower than that of the normal tissues (pH=7.2–7.4). Moreover the endosomes and lysosomes show lower pH levels (pH<6.0)[58]. This difference in pH can be utilized for degrading the main structure of NMs.

pH-induced hydrolysis degradation

In the previous years, a great number of biodegradable polymer-like poly(lactic acid) (PLA), poly(glycolic acid) (PGA), poly(ε-caprolactone) (PCL), and poly(lactic-co-glycolic) (PLGA) were approved by the FDA for *in vivo* application[59]. These acid-labile groups, similar to ester and anhydride, can be introduced in polymeric matrices to

modify the chain degradation. Under acidic environment, these groups can undergo hydrolysis of their ester bonds, and the remaining moieties can be metabolized by the normal acid cycle. Because these biodegradable polymers generally cannot intrinsically absorb light in the NIR region, some researchers have devoted extensive efforts to integrate these polymers to PTAs in order to enhance absorption in the NIR region. Zheng et al.[60] developed a single-step sonication method to entrap the ICG within the PLGA-lipid NPs for *in vivo* tumor-targeting imaging. They then expanded the PLGA-lipid NPs to incorporate doxorubicin (DOX) and ICG simultaneously for combined chemo-photothermal therapy[61]. They noted that the fluorescence of ICG-PLGA-lipid NPs could facilitate the visualization of *in vivo* metabolic distribution[62].

In another work, Tam et al.[63] and Murthy et al.[64] produced a certain type of biodegradable plasmonic nanoclusters through linking several ~4 nm gold particles (AuNPs) using degradable polymers. This degradable linkers are triblock copolymers, also known as PLA(2K)-b-PEG(10K)-b-PLA(2K), which can be degraded under low pH level to release the primary AuNPs (**Figure 4A**). Specifically, lysine/citrate-capped AuNPs mixed with PLA(2K)-b-PEG(10K)-b-PLA(2K) gradually coagulated and aggregated, thus forming a considerably large cluster during solvent evaporation (**Figure 4B**). Their corresponding localized surface plasma resonance (LSPR) spectra showed a red shift as the interparticle spaces between the AuNPs decreased. This approach facilitated the control of the nanocluster size and the optical properties by turning particle volume fractions[65].

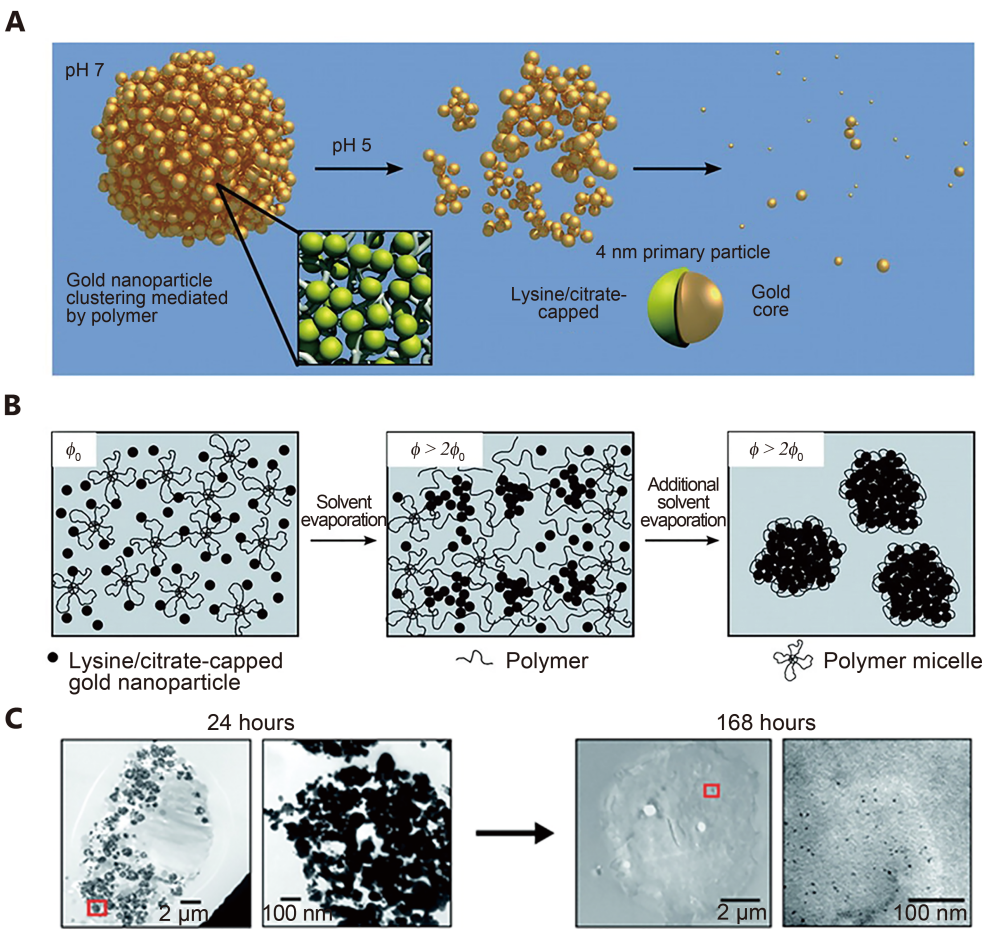

Figure 4 (A) Illustration of the pH-catalyzing degradation of polymer linkers in gold nanoclusters producing primary gold particles (~4 nm). (B) Illustration of the formation process of gold nanoclusters through the assembled 4 nm gold nanoparticle polymer. Particle volume fraction (φ) increases during solvent evaporation. (C) TEM images of cells treated with gold nanoclusters at 24 h and 168 h. The left is at low magnification (scale bar 2 μm) and right is at high magnification (scale bar 100 nm). The right images show the magnified images of the red boxes in the left images. Reproduced with permission from Ref. 63. Copyright 2010 American Chemical Society.

The resulted nanocluster reverted into the original ~4 nm at pH 5, and the associated extinction spectra also reverted to the constituent ligand-capped AuNPs. Similar results were observed in macrophage cells. Particularly, small particles less than 5 nm in diameter appeared in the cells after 168 h (**Figure 4C**). This degradable nanocluster showed enormous potential for PTT, and was later applied in photoacoustic imaging[66].

pH-induced oxidization degradation

pH-dependent oxidization degradation was recently found in some inorganic NMs that underwent low-valence state-oxidized state transition. In 2016, Song et al.[67] found MoOx-PEG has a unique pH-dependent degradation process because it can retain its stability in an acidic environment, and quickly degrades at physiological pH. X-ray photoelectron spectroscopy (XPS) showed that most of the Mo^{V} in the initial MoOx-PEG was oxidized into Mo^{VI} after incubation in PBS (pH=7.4) for 24 h. Based on their LSPR absorption measurements, and their obtained small-angle X-ray diffraction and TEM images, they proposed that MoOx-PEG suffered oxidization degradation. The *in vivo* degradation behaviors observed in Liu's study supported this result. After IV injection of MoOx-PEG (20 mg/kg), it took 7 days to finish the clearance in both the renal and fecal pathways. When exposed to laser light (808 nm, 0.7 W/cm^2), the IV injected MoOx-PEG efficiently ablated the tumors without recurrence within 16 days. Song et al.[67] considered that MoOx-PEG suffered gradual oxidation resulting in production of $[Mo^{VI}O_4]^{2-}$ ions or ultra-small NPs, which facilitate renal clearance. Interestingly, MoOx-PEG removal process did not cause toxicity both *in vitro* and *in vivo*.

Another example of pH-dependent oxidization degradation was found in the ultrasmall Cu_3BiS_3 nanodots (NDs) which were developed by the group of Chen (**Figure 5A**)[68]. Cu_3BiS_3 NDs as copper chalcogenides were observed to have high NIR absorption and suitable for PTT. Under an 880 nm laser light (1 W/cm^2) irradiation for 10 min, 4T1 tumor-bearing mice that received Cu_3BiS_3 NDs (IV injection of 20 mg/kg) exhibited complete tumor ablation (**Figure 5B**).

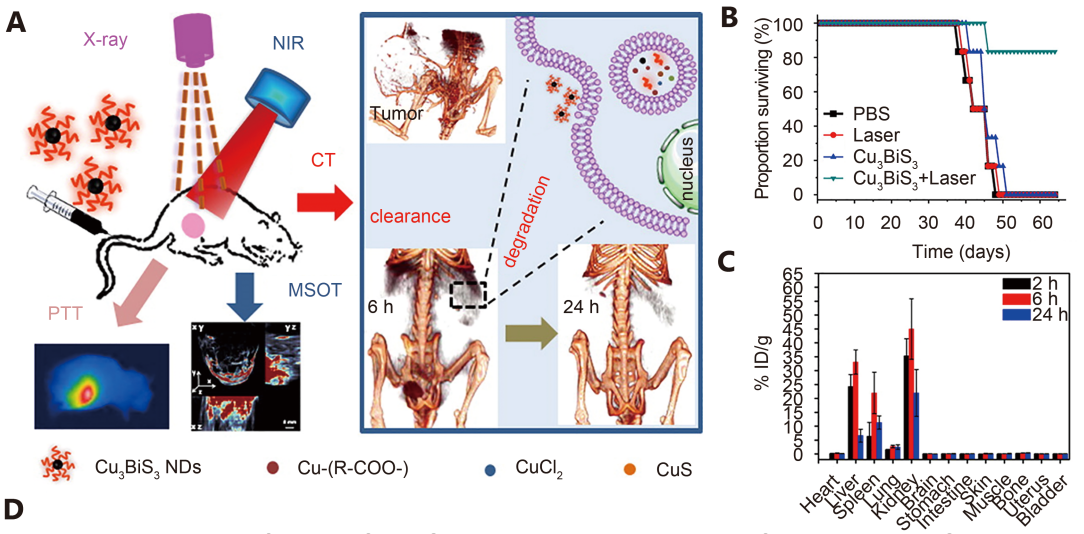

Table 1. Time-Dependent Changes in Copper Species in ALF and DI Water Based on Copper K-Edge XANES

	chemical forms and ratio (%)						
	Cu_2S	CuS	$CuCl_2$	CuCl	Cu-(R-COO-)	CuO	Cu foil
Cu_3BiS_3 NDs	100	0	0	0	0	0	0
ALF 30 min	40	0	0	22.5	37.5	0	0
ALF 12 h	37.4	0	0	17.9	44.7	0	0
ALF 24 h	0	2.5	6.7	0	90.8	0	0
DI water 2 months	20.6	12.6	0	0	46.7	20	0

Figure 5 (A) Illustration of the acid-catalyzing degradation of ultrasmall Cu_3BiS_3 NDs in lysosome promoting renal clearance. These Cu_3BiS_3 NDs can effectively kill cancer cells under multispectral optoacoustic tomography (MSOT) and X-ray computed tomography (CT). (B) Survival proportion of the tumor-bearing mice after various treatments. (C) Tissue biodistribution of Cu_3BiS_3 NDs in balb/c mice at different times. (D) The copper species in ALF and deionized water at different time points characterized by X-ray absorption near-edge structure (XANES). Reproduced with permission from Ref. 68. Copyright 2016 American Chemical Society.

These synthetic Cu_3BiS_3 NDs had a diameter of 10 nm and were almost cleared through renal filtration and urinary excretion at the 24th hour post-injection (**Figure 5C**). In addition to renal clearance of Cu_3BiS_3 NDs, Liu et al.[68] proposed that the Cu_3BiS_3 NDs can undergo oxidation and transformation in the artificial lysosomal fluid (ALF). Synchrotron radiation-based X-ray absorption near-edge structure showed that the Cu_3BiS_3 NDs transformed into 90.8% oxidized species after incubation in the ALF (pH=4.5) for 24 h (**Figure 5D**). This rapid and thorough degradation and clearance process greatly reduced the potential toxicity. Histological examination and blood biochemistry showed that Cu_3BiS_3 at a certain dose did not cause toxicity *in vivo*.

NIR laser-induced degradation

Laser irradiation is the basic condition in PTT and it may cause structural damage that accelerates the metabolism of NMs. As discussed in the previous section, the degradation of the developed biodegradable plasmonic nanoclusters by Yoon et al.[69] was laser-fluence-dependent. When laser fluence exceeded 8 mJ/cm^2, 130 nm nanoclusters showed certain changes in the absorbance spectra. This change was more evident when laser fluence exceeded 20 mJ/cm^2. Yoon et al.[69] owed this spectral change to the morphological change. This characteristic is to the reshaping of gold nanorods after laser irradiation[70]. This light stability was also highly dependent on material composition and binding forces. For liposome-gold clusters, Rengan et al.[36] found that 1,2-distearoyl-sn-glycero-3-phosphocholine (DSPC) based liposome-gold clusters disassembled into small gold particles of ~5 nm after 20 min of laser irradiation (750 nm, 650 mW). Furthermore, 7.5 min of laser irradiation (750 nm, 650 mW) was sufficient for killing the MDA-MB-231 cells. In another study, NIR light excitation (2.0 W/cm^2, 40 s) triggered the disintegration of the hollow copper sulfide nanoparticles (HCuSNPs) into small CuS NPs (7–12 nm) because of the polycrystalline CuS of the shells. This laser-triggered disintegration of HCuSNPs accelerated their elimination from the tumors. Quantitative analysis showed approximately 21% ID of Cu was removed from the tumors while it was increased to ~47% ID under laser treatment within 14 days. Owing to this unique feature, a NIR light-transformable nanocomposite was constructed by assembling cytosine-guanine (CpG) on chitosan-coated HCuSNPs. The nanocomposite was then used for photothermal and immune combined cancer therapy[71].

Recently, the self-assembly of the amphiphilic block copolymer-tethered AuNPs provide a versatile approach to develop novel biodegradable polymer/AuNPs assemblies for PTT[72]. When amphiphilic block copolymers show structural damage or change *in vivo*, the building blocks dissociate into their original sizes, thereby facilitating their elimination from the body. The main assemblage methods are the film rehydration method and the selective solvent method that closely packs AuNPs, which turn LSPR peaks in the NIR region[73,74]. In 2015, Deng et al.[75] applied this method to produce biocompatible gold nanomicelles based on amphipathic polymer (p-(MEO_2MA-co-(HEMA-gPCL))-tethered AuNPs. The amphipathic polymer was terminated with the mercapto groups, thereby forming a comb shape, which could pack more AuNPs and could generate ultrastrong plasmonic coupling. When exposed to NIR laser (808 nm, 1.5 W/cm^2) for 5 min, 0.2 mg/mL of the gold nanomicelle solution can be heated to 57 °C. After NIR laser irradiation, each nanomicelle dissociate into a small size of 6 nm, as proven by the TEM images. This phenomenon was later demonstrated *in vivo*. The nanomicelles showed no observable toxicity even at high incubation concentrations, but the dissociated AuNPs were not rapidly eliminated through renal activity[75].

Degradation induced by other factors

In addition to the above-defined stimulus, some PTAs with degradation mechanisms that are still unknown or not proven are reviewed in this section. For example, systemically administered IONPs are first absorbed by the mononuclear phagocytic system of the liver and the spleen and then degraded into Fe ions by lysosomes. The degraded irons are then retained in storage proteins or are eliminated from the body through the typical iron metabolic pathways[76-78]. Currently, IONPs are extensively applied in biomedicine, particularly in magnetic resonance imaging (MRI), drug delivery, and hyperthermia treatment[79].

Chen et al.[80] reported that a certain type of highly crystallized IONPs (HCIONPs) coated with a polysiloxane-containing diblock copolymer is an effective and biodegradable mediator for PTT. These HCIONPs synthesized by thermal decomposition with certain modifications have a desirable plane orientation that can induce photothermal effect. When exposed to NIR irradiation (885 nm, 2.5 W/cm^2), the HCIONP solution (0.5 mg/mL, Fe) produced a considerably higher temperature (33 °C) than pure water (3 °C). *In vivo* tumor photothermal therapy was further examined through intravenously administered HCIONPs, and the SUM-159 tumor completely regressed under the same laser irradiation

parameters. Moreover, the copolymer coating did not change the biodegradability of the IONPs, as indicated by the inductively coupled plasma mass spectrometry (ICP-MS), which showed the absence of significant difference in the iron concentrations of the organs between the HCIONPs-treated mice and the controlled, mice after photothermal therapy. The hematoxylin- and eosin-stained main organs also suggested that the injected HCIONPs did not cause evident tissue damage in mice[80].

Iron-oxide nanoparticles can integrate with PTAs to improve their photothermal efficiency for PTT. Ma et al.[81] developed a biodegradable nanocomposite based on 1,2-distearoylsn-glycero-3-phosphoethanolamine-N-methoxy (polyethylene glycol) (DSPE-PEG) coated superparamagnetic iron oxide (SPIO) nanoparticles encapsulating ICG molecules (SPIO@DSPE-PEG/ICG NPs). The resulting SPIO@DSPE-PEG/ICG NPs can maintain the biodegradability of the IONPs and possess high photothermal conversion efficiency. Under NIR laser irradiation, the SPIO@DSPE-PEG/ICG can induce intense temperature elevation, which can be observed in *in vitro* and *in vivo* photothermal therapy[81]. Recently, IONPs enveloped by conjugated polymers have been reported to improve photothermal efficiency[82,83]. Although these nanostructures have been applied successfully in PTT, and have exhibited low toxicity *in vitro* and *in vivo*, information on their biodegradability, metabolic pathway, and long-term toxicology is limited[84].

CuS NPs are recognized as alternatives to gold nanostructures in PTT because of their low toxicity and strong NIR absorption[85,86]. Copper is an essential element in human health, and excess copper in the body is mainly excreted through bile to maintain balance[87]. As physicochemical properties affect NMs uptake, transport, and fate *in vivo*, CuS can be metabolized in humans through smart manipulation of their physicochemical properties. In 2013, Guo et al.[88] reported a biodegradable hollow CuS nanoparticle that can be eliminated through hepatobiliary and renal excretion. They proposed the systemically injected PEGylated HCuSNPs accumulated in major organs in which the HCuSNPs split into small CuSNPs and dissociated Cu ions. The hepatobiliary elimination and renal excretion of Cu ions accounted for the 67% ID and the 23 % ID, respectively, within the 1st month of post-injection. After demonstrating the biodegradability of HCuSNPs, they further examined the cytotoxicity of PEG-HCuSNPs. Their results showed that PEG-HCuSNPs had low toxicity at a concentration of 100 μg/mL on RAW 264.7 cells, and the results could be related to the released Cu ions from the CuS[88].

Targeting delivery of biodegradable PTAs

The newly developed biodegradable PTAs are usually delivered to cancer tissues through passive targeting, which is driven by the enhanced permeability and retention (EPR) effect[89]. As the blood vessels of the tumors are abnormal hyperplasias[90], with wider space in their vascular walls[91] and with incomplete structures, biodegradable PTAs in the bloodstream can extravasate from leaky vessels into the tumor interstitium. To strengthen the EPR effect, the size of the biodegradable PTAs should be maintained within the range of 60 nm to 400 nm[92], and the surface of the biodegradable PTAs generally function with PEG to create a hydrophilic protective layer and prolong the blood circulation time. For example, PEG modification increases the blood circulation half-life of Doxil from 30 min to 80 h. Moreover, small NPs show higher tumor penetration efficiency than large NPs[93], but they can be cleared away from the tumor through the lymphatic drainage[94].

Ligand-mediated active targeting provides another way to increase the accuracy of the targeting PTAs, which mainly takes advantage of targeting specific antigens or receptors on the surface of tumor cells, in the cancer tissues[95]. Generally, PTAs are conjugated with the corresponding ligands, such as proteins, peptides, aptamers, and small molecules through physical and chemical binding. Our study demonstrated that the uptake of transferrin-conjugated gold nanoshells in MCF-7 cells was 15-fold higher than that of the nonconjugated gold nanoshells[17]. Moreover, PTAs with magnetic properties can deliver to the tumor tissue under the guidance of external magnetic field[96].

In addition, the cellular internalization of the PTAs is critical in the enhancement of tumor-targeted delivery[97]. Thus, considerable attention is necessary for improvement of the cellular internalization of PTAs through the optimization of their physicochemical properties. For example, NP size can affect the efficiency and the pathway of the cellular uptake[98]. Zhao et al.[62] reported that the cell uptake of ICG-loaded polymer-lipid NPs varied with size, and the NPs with 39 nm size were the most absorbed by tumor cells among the 39 nm, 68 nm, and 116 nm NPs observed. Moreover, NPs with diameters of <200 nm were internalized into cells through clathrin-coated pits. When the size of the NP increases, caveolae-mediated internalization is apparent, and turned into the predominant pathway where 500 nm NPs enter[99].

Clearance of biodegradable PTAs

Biodegradation of PTAs undergoes a two-step process:

degradation and clearance. The clearance pathway of the biodegradable PTAs mainly includes the hepatic clearance and the renal clearance, which are primarily determined by particle size. NMs larger than 10 nm are immediately trapped by reticuloendothelial systems (RES) of the liver and spleen[100]. NMs smaller than 5.5 nm are immediately filtered from the blood by the kidney[25].

Hepatic clearance of biodegradable PTAs

As the systemically administered PTAs are mostly aggregated and retained in the liver, the hepatic clearance of PTAs is the main metabolic pathway and also related to PTAs' size. PTAs with size less than ~200 nm tend to be cleaned by hepatocytes or to enter the lymphatic circulation, whereas PTAs with size large than ~200 nm are effectively absorbed by the Kupffer cells[101]. The exact clearance mechanism is dependent on the interactions between the PTAs and the intracellular components. Lysosome-mediated degradation, which is the dominant pathway of clearance for the PTAs in the Kupffer cells, is associated with the acid hydrolase enzymes and the acidic microenvironment. For example, lysosomal metabolism of IONPs is relevant to lysosomal α-glucosidase[102], low pH, and chelates[103]. The hepatic biodegradation capacity is notably limited and excessive accumulation of biodegradable PTAs can cause cytotoxicity.

Renal clearance of biodegradable PTAs

For the inert PTAs that cannot be easily metabolized by the liver, developing cleavable or decomposable PTAs for renal clearance is an effective strategy. Renal clearance first involves glomerular filtration that directly affects renal clearance capability. As the filtration-size threshold is ~5.5 nm[25], NPs smaller than 5.5 nm can be effectively excreted in the urine. NPs larger than 5.5 nm likely shift to the liver. Deng et al.[75] developed a type of cleavable gold clusters that can decompose into small gold particles (~6 nm). These decomposed AuNPs can be subsequently eliminated through the renal pathway. Quantitative analysis of urine indicated that a 4% dose of elemental Au was cleared on day 7. However, Park et al.[104,105] found that the PLGA-gold nanoshells were not excreted effectively through the kidneys because the remaining AuNPs retained large sizes. Certain ultrasmall NPs (<10 nm) are among example of renal clearable inorganic NPs[106,107]. In contrast to biodegradable PTAs, ultrasmall PTAs were rapidly eliminated by the kidneys without undergoing the degradation process. This may weaken the EPR-mediated delivery of PTAs to the cancer cells, thus it could influence the treatment effect of PTT.

Conclusions

Biodegradability has been demonstrated as the key avenue regarding the issue on safety of NMs. In this review, different stimuli-responsive PTAs are presented, and their considered design, degradation behavior, and excretion pathway are discussed. However, limitations and challenges with regard to PTAs still exist.

Current evaluation methods for biocompatibility are mostly focused on acute toxicity. However, long-term toxicity and aberrant cellular responses without toxicity necessitate further evaluation. The aberrant cellular responses include the oxidative stress, DNA damage, abnormal enzyme activity, mitochondrial membrane dysfunction, and changes in gene expression[13]. Furthermore, the consistent criteria and decision method have not been established for biodegradability *in vivo*. Further understanding on the detailed biodegradation mechanisms, metabolic pathway, and toxicity assessment of inorganic NMs are still progressing. Developing biodegradable PTAs are preferentially based on safe and extensively studied biodegradable materials, such as liposome, polyester, and natural macromolecule.

At present, injected PTAs are mostly dependent on the passive target in the tumor via EPR. Unpredictable degradation of NMs can happen during blood circulation. Therefore, the ideal PTAs should be bioinert and stable in biological environment and can be immediately excreted after carrying out their function. Furthermore, enhanced tumor retention, penetration, cellular internalization, and nuclear uptake of PTAs should be considered. Combination of multi-mode targeting and stimuli-responsive PTAs is a promising direction to attain controllable degradation rates. With the development of programmed biodegradable PTAs, we believe that PTT can be soon translated to clinical applications.

Conflict of interest statement

No potential conflicts of interest are disclosed.

References

1. O'Neal DP, Hirsch LR, Halas NJ, Payne JD, West JL. Photo-

thermal tumor ablation in mice using near infrared-absorbing nanoparticles. Cancer Lett. 2004; 209: 171-6.

2. Liu H, Chen D, Li L, Liu T, Tan L, Wu X, et al. Multifunctional gold nanoshells on silica nanorattles: a platform for the combination of photothermal therapy and chemotherapy with low systemic toxicity. Angew Chem Int Ed. 2011; 123: 921-5.
3. Zhang Z, Wang J, Nie X, Wen T, Ji Y, Wu X, et al. Near infrared laser-induced targeted cancer therapy using thermoresponsive polymer encapsulated gold nanorods. J Am Chem Soc. 2014;136:7317-26.
4. Fu C, He C, Tan L, Wang S, Shang L, Li L, et al. High-yield preparation of robust gold nanoshells on silica nanorattles with good biocompatiblity. Sci Bull. 2016; 61: 282-91.
5. Yang K, Xu H, Cheng L, Sun C, Wang J, Liu Z. In vitro and in vivo near-infrared photothermal therapy of cancer using polypyrrole organic nanoparticles. Adv Mater. 2012; 24: 5586-92.
6. Yang J, Choi J, Bang D, Kim E, Lim EK, Park H, et al. Convertible organic nanoparticles for near-infrared photothermal ablation of cancer cells. Angew Chem Int Ed. 2011; 50: 441-4.
7. Wang S, Shang L, Li L, Yu Y, Chi C, Wang K, et al. Metal-organic-framework-derived mesoporous carbon nanospheres containing porphyrin-like metal centers for conformal phototherapy. Adv Mater. Published online first: July 27, 2016. DOI: 10.1002/adma.201602197.
8. Yang K, Zhang S, Zhang G, Sun X, Lee S-T, Liu Z. Graphene in mice: ultrahigh in vivo tumor uptake and efficient photothermal therapy. Nano Lett. 2010; 10: 3318-23.
9. Tian Q, Tang M, Sun Y, Zou R, Chen Z, Zhu M, et al. Hydrophilic flower-like CuS superstructures as an efficient 980 nm laser-driven photothermal agent for ablation of cancer cells. Adv Mater. 2011; 23: 3542-47.
10. Li W, Zamani R, Rivera Gil P, Pelaz B, Ibáñez M, Cadavid D, et al. CuTe nanocrystals: shape and size control, plasmonic properties, and use as SERS probes and photothermal agents. J Am Chem Soc. 2013; 135: 7098-101.
11. Chen G, Zhou J, Zuo J, Yang Q. Organometallically anisotropic growth of ultra-long Sb_2Se_3 nanowires with highly enhanced photothermal response. ACS Appl Mater Interfaces. 2016; 8: 2819-25.
12. Li KC, Chu HC, Lin Y, Tuan HY, Hu YC. PEGylated copper nanowires as a novel photothermal therapy agent. ACS Appl Mater Interfaces. 2016; 8: 12082-90.
13. Singh N, Jenkins GJ, Asadi R, Doak SH. Potential toxicity of superparamagnetic iron oxide nanoparticles (SPION). Nano Rev. 2010; 1: 5358.
14. Langer R. Drug delivery and targeting. Nature. 1998; 392: 5-10.
15. Qu G, Bai Y, Zhang Y, Jia Q, Zhang W, Yan B. The effect of multiwalled carbon nanotube agglomeration on their accumulation in and damage to organs in mice. Carbon. 2009; 47: 2060-9.
16. Liu H, Liu T, Wang H, Li L, Tan L, Fu C, et al. Impact of PEGylation on the biological effects and light heat conversion efficiency of gold nanoshells on silica nanorattles. Biomaterials. 2013; 34: 6967-75.
17. Liu H, Liu T, Wu X, Li L, Tan L, Chen D, et al. Targeting gold nanoshells on silica nanorattles: a drug cocktail to fight breast tumors via a single irradiation with near-infrared laser light. Adv Mater. 2012; 24: 755-61.
18. Choi HS, Liu W, Misra P, Tanaka E, Zimmer JP, Ipe BI, et al. Renal clearance of quantum dots. Nat Biotechnol. 2007; 25: 1165-70.
19. Ma N, Li Y, Xu H, Wang Z, Zhang X. Dual redox responsive assemblies formed from diselenide block copolymers. J Am Chem Soc. 2010; 132: 442-3.
20. Jiang J, Tong X, Zhao Y. A new design for light-breakable polymer micelles. J Am Chem Soc. 2005; 127: 8290-1.
21. Delplace V, Nicolas J. Degradable vinyl polymers for biomedical applications. Nature Chem. 2015; 7: 771-84.
22. Ehlerding EB, Chen F, Cai W. Biodegradable and renal clearable inorganic nanoparticles. Adv Sci. 2016; 3: 1500223 (1-8).
23. Wang PC, Shan L. Essential elements to consider for MRI cell tracking studies with iron oxide-based labeling agents. J Basic Clin Med. 2012; 1: 1-6.
24. Park JH, Gu L, Von Maltzahn G, Ruoslahti E, Bhatia SN, Sailor MJ. Biodegradable luminescent porous silicon nanoparticles for in vivo applications. Nature Mater. 2009; 8: 331-6.
25. Zhou C, Long M, Qin Y, Sun X, Zheng J. Luminescent gold nanoparticles with efficient renal clearance. Angew Chem. 2011; 123: 3226-30.
26. Cheng L, Wang C, Feng L, Yang K, Liu Z. Functional nanomaterials for phototherapies of cancer. Chem Rev. 2014; 114: 10869-939.
27. Davidsen J, Vermehren C, Frokjaer S, Mouritsen OG, Jørgensen K. Drug delivery by phospholipase A_2 degradable liposomes. Int J Pharm. 2001; 214: 67-9.
28. Lucky SS, Soo KC, Zhang Y. Nanoparticles in photodynamic therapy. Chem Rev. 2015; 115: 1990-2042.
29. Yuan A, Tang X, Qiu X, Jiang K, Wu J, Hu Y. Activatable photodynamic destruction of cancer cells by NIR dye/photosensitizer loaded liposomes. Chem Commun. 2015; 51: 3340-2.
30. Suganami A, Toyota T, Okazaki S, Saito K, Miyamoto K, Akutsu Y, et al. Preparation and characterization of phospholipid-conjugated indocyanine green as a near-infrared probe. Bioorg Med Chem Lett. 2012; 22: 7481-5.
31. Lovell JF, Jin CS, Huynh E, Jin H, Kim C, Rubinstein JL, et al. Porphysome nanovesicles generated by porphyrin bilayers for use as multimodal biophotonic contrast agents. Nature Mater. 2011; 10: 324-32.
32. Jin CS, Lovell JF, Chen J, Zheng G. Ablation of hypoxic tumors with dose-equivalent photothermal, but not photodynamic, therapy using a nanostructured porphyrin assembly. ACS Nano. 2013; 7: 2541-50.
33. Lovell JF, Jin CS, Huynh E, MacDonald TD, Cao W, Zheng G. Enzymatic regioselection for the synthesis and biodegradation of porphysome nanovesicles. Angew Chem Int Ed. 2012; 51: 2429-

33.
34. Troutman TS, Barton JK, Romanowski M. Biodegradable plasmon resonant nanoshells. Adv Mater. 2008; 20: 2604-8.
35. Rengan AK, Bukhari AB, Pradhan A, Malhotra R, Banerjee R, Srivastava R, et al. In vivo analysis of biodegradable liposome gold nanoparticles as efficient agents for photothermal therapy of cancer. Nano Lett. 2015; 15: 842-8.
36. Rengan AK, Jagtap M, De A, Banerjee R, Srivastava R. Multifunctional gold coated thermo-sensitive liposomes for multimodal imaging and photo-thermal therapy of breast cancer cells. Nanoscale. 2014; 6: 916-23.
37. Leung SJ, Kachur XM, Bobnick MC, Romanowski M. Wavelength-selective light-Induced release from plasmon resonant liposomes. Adv Funct Mater. 2011; 21: 1113-21.
38. Leung SJ, Romanowski M. NIR-activated content release from plasmon resonant liposomes for probing single-cell responses. ACS Nano. 2012; 6: 9383-91.
39. Allen BL, Kichambare PD, Gou P, Vlasova , Kapralov AA, Konduru N, et al. Biodegradation of single-walled carbon nanotubes through enzymatic catalysis. Nano Lett. 2008; 8: 3899-903.
40. Allen BL, Kotchey GP, Chen Y, Yanamala NV, Klein-Seetharaman J, Kagan VE, et al. Mechanistic investigations of horseradish peroxidase-catalyzed degradation of single-walled carbon nanotubes. J Am Chem Soc. 2009; 131: 17194-205.
41. Kagan VE, Konduru NV, Feng W, Allen BL, Conroy J, Volkov Y, et al. Carbon nanotubes degraded by neutrophil myeloperoxidase induce less pulmonary inflammation. Nature Nanotech. 2010; 5: 354-9.
42. Shvedova AA, Kapralov AA, Feng WH, Kisin ER, Murray AR, Mercer RR, et al. Impaired clearance and enhanced pulmonary inflammatory/fibrotic response to carbon nanotubes in myeloperoxidase-deficient mice. PLoS one. 2012; 7: e30923.
43. Bhattacharya K, Andón FT, El-Sayed R, Fadeel B. Mechanisms of carbon nanotube-induced toxicity: focus on pulmonary inflammation. Adv Drug Deliv Rev. 2013; 65: 2087-97.
44. Elgrabli D, Dachraoui W, Ménard-Moyon C, Liu XJ, Bégin D, Bégin-Colin S, et al. Carbon nanotube degradation in macrophages: live nanoscale monitoring and understanding of biological pathway. ACS Nano. 2015; 9: 10113-24.
45. Nunes A, Bussy C, Gherardini L, Meneghetti M, Herrero MA, Bianco A, et al. In vivo degradation of functionalized carbon nanotubes after stereotactic administration in the brain cortex. Nanomedicine. 2012; 7: 1485-94.
46. Bussy C, Hadad C, Prato M, Bianco A, Kostarelos K. Intracellular degradation of chemically functionalized carbon nanotubes using a long-term primary microglial culture model. Nanoscale. 2016; 8: 590-601.
47. Zhao Y, Allen BL, Star A. Enzymatic degradation of multiwalled carbon nanotubes. J Phys Chem A. 2011; 115: 9536-44.
48. Zhou F, Xing D, Ou Z, Wu B, Resasco DE, Chen WR. Cancer photothermal therapy in the near-infrared region by using single-walled carbon nanotubes. J Biomed Opt. 2009; 14: 021009 (1-7).
49. Kim JW, Galanzha EI, Shashkov EV, Moon H-M, Zharov VP. Golden carbon nanotubes as multimodal photoacoustic and photothermal high-contrast molecular agents. Nature Nanotech. 2009; 4: 688-94.
50. Markovic ZM, Harhaji-Trajkovic LM, Todorovic-Markovic BM, Kepić DP, Arsikin KM, Jovanović SP, et al. In vitro comparison of the photothermal anticancer activity of graphene nanoparticles and carbon nanotubes. Biomaterials. 2011; 32: 1121-9.
51. Liu X, Tao H, Yang K, Zhang S, Lee ST, Liu Z. Optimization of surface chemistry on single-walled carbon nanotubes for in vivo photothermal ablation of tumors. Biomaterials. 2011; 32: 144-51.
52. Wang X, Wang C, Cheng L, Lee ST, Liu Z. Noble metal coated single-walled carbon nanotubes for applications in surface enhanced Raman scattering imaging and photothermal therapy. J Am Chem Soc. 2012; 134: 7414-22.
53. Robinson JT, Welsher K, Tabakman SM, Sherlock SP, Wang H, Luong R, et al. High performance in vivo near-IR (>1 μm) imaging and photothermal cancer therapy with carbon nanotubes. Nano Res. 2010; 3: 779-93.
54. Kotchey GP, Allen BL, Vedala H, Yanamala N, Kapralov AA, Tyurina YY, et al. The enzymatic oxidation of graphene oxide. ACS Nano. 2011; 5: 2098-108.
55. Girish CM, Sasidharan A, Gowd GS, Nair S, Koyakutty M. Confocal raman imaging study showing macrophage mediated biodegradation of graphene in vivo. Adv Healthcare Mater. 2013; 2: 1489-1500.
56. Li Y, Feng L, Shi X, Wang X, Yang Y, Yang K, et al. Surface coating-dependent cytotoxicity and degradation of graphene derivatives: towards the design of non-toxic, degradable nano-graphene. Small. 2014; 10: 1544-54.
57. Xiong H, Guo Z, Zhang W, Zhong H, Liu S, Ji Y. Redox-responsive biodegradable PEGylated nanographene oxide for efficiently chemo-photothermal therapy: A comparative study with non-biodegradable PEGylated nanographene oxide. J Photochem Photobiol B. 2014; 138: 191-201.
58. Padilla-Parra S, Matos PM, Kondo N, Marin M, Santos NC, Melikyan GB. Quantitative imaging of endosome acidification and single retrovirus fusion with distinct pools of early endosomes. Proc Natl Acad Sci U S A. 2012; 109: 17627-32.
59. Oliveira MF, Guimarães PP, Gomes AD, Suárez D, Sinisterra RD. Strategies to target tumors using nanodelivery systems based on biodegradable polymers, aspects of intellectual property, and market. J Chem Biol. 2013; 6: 7-23.
60. Zheng C, Zheng M, Gong P, Jia D, Zhang P, Shi B, et al. Indocyanine green-loaded biodegradable tumor targeting nanoprobes for in vitro and in vivo imaging. Biomaterials. 2012; 33: 5603-9.
61. Zheng M, Yue C, Ma Y, Gong P, Zhao P, Zheng C, et al. Single-step assembly of DOX/ICG loaded lipid-polymer nanoparticles for highly effective chemo-photothermal combination therapy. ACS Nano. 2013; 7: 2056-67.
62. Zhao P, Zheng M, Yue C, Luo Z, Gong P, Gao G, et al. Improving drug accumulation and photothermal efficacy in tumor

depending on size of ICG loaded lipid-polymer nanoparticles. Biomaterials. 2014; 35: 6037-46.

63. Tam JM, Tam JO, Murthy A, Ingram DR, Ma LL, Travis K, et al. Controlled assembly of biodegradable plasmonic nanoclusters for near-infrared imaging and therapeutic applications. ACS Nano. 2010; 4: 2178-84.
64. Murthy AK, Stover RJ, Borwankar AU, Nie GD, Gourisankar S, Truskett TM, et al. Equilibrium gold nanoclusters quenched with biodegradable polymers. ACS Nano. 2012; 7: 239-51.
65. Tam JM, Murthy AK, Ingram DR, Nguyen R, Sokolov KV, Johnston KP. Kinetic assembly of near-IR-active gold nanoclusters using weakly adsorbing polymers to control the size. Langmuir. 2010; 26: 8988-99.
66. Yoon SJ, Mallidi S, Tam JM, Tam JO, Murthy A, Johnston KP, et al. Utility of biodegradable plasmonic nanoclusters in photoacoustic imaging. Opt Lett. 2010; 35: 3751-3.
67. Song G, Hao J, Liang C, Liu T, Gao M, Cheng L, et al. Degradable molybdenum oxide nanosheets with rapid clearance and efficient tumor homing capabilities as a therapeutic nanoplatform. Angew Chem Int Ed. 2016; 55: 2122-6.
68. Liu J, Wang P, Zhang X, Wang L, Wang D, Gu Z, et al. Rapid degradation and high renal clearance of Cu_3BiS_3 nanodots for efficient cancer diagnosis and photothermal therapy in vivo. ACS Nano. 2016; 10: 4587-98.
69. Yoon SJ, Murthy A, Johnston KP, Sokolov KV, Emelianov SY. Thermal stability of biodegradable plasmonic nanoclusters in photoacoustic imaging. Opt Express. 2012; 20: 29479-87.
70. Wang Y, Teitel S, Dellago C. Surface-driven bulk reorganization of gold nanorods. Nano Lett. 2005; 5: 2174-8.
71. Guo L, Yan DD, Yang D, Li Y, Wang X, Zalewski O, et al. Combinatorial photothermal and immuno cancer therapy using chitosan-coated hollow copper sulfide nanoparticles. ACS Nano. 2014; 8: 5670-81.
72. Song J, Huang P, Duan H, Chen X. Plasmonic vesicles of amphiphilic nanocrystals: optically active multifunctional platform for cancer diagnosis and therapy. Acc Chem Res. 2015; 48: 2506-15.
73. Huang P, Lin J, Li W, Rong P, Wang Z, Wang S, et al. Biodegradable gold nanovesicles with an ultrastrong plasmonic coupling effect for photoacoustic imaging and photothermal therapy. Angew Chem Int Ed. 2013; 52: 13958-64.
74. Deng H, Zhong Y, Du M, Liu Q, Fan Z, Dai F, et al. Theranostic self-assembly structure of gold nanoparticles for NIR photothermal therapy and X-Ray computed tomography imaging. Theranostics. 2014; 4: 904-18.
75. Deng H, Dai F, Ma G, Zhang X. Theranostic gold nanomicelles made from biocompatible comb-like polymers for thermochemotherapy and multifunctional imaging with rapid clearance. Adv Mater. 2015; 27: 3645-53.
76. Weissleder Ra, Stark D, Engelstad B, Bacon B, Compton C, White D, et al. Superparamagnetic iron oxide: pharmacokinetics and toxicity. AJR Am J Roentgenol. 1989; 152: 167-73.
77. Pouliquen D, Le Jeune J, Perdrisot R, Ermias A, Jallet P. Iron oxide nanoparticles for use as an MRI contrast agent: pharmacokinetics and metabolism. Magn Reson Imaging. 1991; 9: 275-83.
78. Briley-Saebo K, Bjørnerud A, Grant D, Ahlstrom H, Berg T, Kindberg GM. Hepatic cellular distribution and degradation of iron oxide nanoparticles following single intravenous injection in rats: implications for magnetic resonance imaging. Cell Tissue Res. 2004; 316: 315-23.
79. Yang F, Jin C, Subedi S, Lee CL, Wang Q, Jiang Y, et al. Emerging inorganic nanomaterials for pancreatic cancer diagnosis and treatment. Cancer Treat Rev. 2012; 38: 566-79.
80. Chen H, Burnett J, Zhang F, Zhang J, Paholak H, Sun D. Highly crystallized iron oxide nanoparticles as effective and biodegradable mediators for photothermal cancer therapy. J Mater Chem B. 2014; 2: 757-65.
81. Ma Y, Tong S, Bao G, Gao C, Dai Z. Indocyanine green loaded SPIO nanoparticles with phospholipid-PEG coating for dual-modal imaging and photothermal therapy. Biomaterials. 2013; 34: 7706-14.
82. Zhang X, Xu X, Li T, Lin M, Lin X, Zhang H, et al. Composite photothermal platform of polypyrrole-enveloped Fe_3O_4 nanoparticle self-assembled superstructures. ACS Appl Mater Interfaces. 2014; 6: 14552-61.
83. Wang C, Xu H, Liang C, Liu Y, Li Z, Yang G, et al. Iron oxide@ polypyrrole nanoparticles as a multifunctional drug carrier for remotely controlled cancer therapy with synergistic antitumor effect. ACS Nano. 2013; 7: 6782-95.
84. Song X, Chen Q, Liu Z. Recent advances in the development of organic photothermal nano-agents. Nano Res. 2015; 8: 340-54.
85. Li Y, Lu W, Huang Q, Li C, Chen W. Copper sulfide nanoparticles for photothermal ablation of tumor cells. Nanomedicine. 2010; 5: 1161-71.
86. Zha Z, Zhang S, Deng Z, Li Y, Li C, Dai Z. Enzyme-responsive copper sulphide nanoparticles for combined photoacoustic imaging, tumor-selective chemotherapy and photothermal therapy. Chem Commun. 2013; 49: 3455-7.
87. Cousins RJ. Absorption, transport, and hepatic metabolism of copper and zinc: special reference to metallothionein and ceruloplasmin. Physiol Rev. 1985; 65: 238-309.
88. Guo L, Panderi I, Yan DD, Szulak K, Li Y, Chen Y-T, et al. A comparative study of hollow copper sulfide nanoparticles and hollow gold nanospheres on degradability and toxicity. ACS Nano. 2013; 7: 8780-93.
89. Matsumura Y, Maeda H. A new concept for macromolecular therapeutics in cancer chemotherapy: Mechanism of tumoritropic accumulation of proteins and the antitumor agent smancs. Cancer Res. 1986; 46: 6387-92.
90. Folkman J. Tumor angiogenesis: Therapeutic implications. N Engl J Med. 1971; 285: 1182-6.
91. Hobbs SK, Monsky WL, Yuan F, Roberts WG, Griffith L, Torchilin VP, et al. Regulation of transport pathways in tumor vessels: Role of tumor type and microenvironment. Proc Natl Acad Sci U S A. 1998; 95: 4607-12.

92. Maeda H, Wu J, Sawa T, Matsumura Y, Hori K. Tumor vascular permeability and the EPR effect in macromolecular therapeutics: a review. J Controlled Release. 2000; 65: 271-84.
93. Tang L, Yang X, Yin Q, Cai K, Wang H, Chaudhury I, et al. Investigating the optimal size of anticancer nanomedicine. Proc Natl Acad Sci U S A. 2014; 111: 15344-9.
94. Pontus K, René in 't Z, Sarah F, Sven-Erik S. Optimizing retention of multimodal imaging nanostructures in sentinel lymph nodes by nanoscale size tailoring. Nanomedicine: NBM. 2014; 10: 1089-95.
95. Huang J, Li Y, Orza A, Lu Q, Guo P, Wang L, et al. Magnetic nanoparticle facilitated drug delivery for cancer therapy with targeted and image-guided approaches. Adv Funct Mater. 2016; 26: 3818-36.
96. Li L, Fu S, Chen C, Wang X, Fu C, Wang S, et al. Microenvironment-driven bioelimination of magnetoplasmonic nanoassemblies and their multimodal imaging-guided tumor photothermal therapy. ACS Nano. 2016; 10: 7094-105.
97. Wang S, Huang P, Chen X. Hierarchical targeting strategy for enhanced tumor tissue accumulation/retention and cellular internalization. Adv Mater. Published online first: June 3, 2016. DOI: 10.1002/adma.201601498.
98. Duan X, Li Y. Physicochemical characteristics of nanoparticles affect circulation, biodistribution, cellular internalization, and trafficking. Small. 2013; 9: 1521-32.
99. Rejman J, Oberle V, Zuhorn IS, Hoekstra D. Size-dependent internalization of particles via the pathways of clathrinand caveolae-mediated endocytosis. Biochem J. 2004; 377: 159-69.
100. Nel A, Xia T, Mädler L, Li N. Toxic potential of materials at the nanolevel. Science. 2006; 311: 622-7.
101. Wang B, He X, Zhang Z, Zhao Y, Feng W. Metabolism of nanomaterials in vivo: Blood circulation and organ clearance. Acc Chem Res. 2013; 46: 761-9.
102. Lunov O, Syrovets T, Röcker C, Tron K, Nienhaus GU, Rasche V, et al. Lysosomal degradation of the carboxydextran shell of coated superparamagnetic iron oxide nanoparticles and the fate of professional phagocytes. Biomaterials. 2010; 31: 9015-22.
103. Arbab AS, Wilson LB, Ashari P, Jordan EK, Lewis BK, Frank JA. A model of lysosomal metabolism of dextran coated superparamagnetic iron oxide (SPIO) nanoparticles: implications for cellular magnetic resonance imaging. NMR Biomed. 2005; 18: 383-9.
104. Park H, Yang J, Seo S, Kim K, Suh J, Kim D, et al. Multifunctional nanoparticles for photothermally controlled drug delivery and magnetic resonance imaging enhancement. Small. 2008; 4: 192-6.
105. Park H, Yang J, Lee J, Haam S, Choi I-H, Yoo K-H. Multifunctional nanoparticles for combined doxorubicin and photothermal treatments. ACS Nano. 2009; 3: 2919-26.
106. Zhou M, Li J, Liang S, Sood AK, Liang D, Li C. CuS Nanodots with ultrahigh efficient renal clearance for positron emission tomography imaging and image-guided photothermal therapy. ACS Nano. 2015; 9: 7085-96.
107. Tang S, Chen M, Zheng N. Sub-10-nm Pd nanosheets with renal clearance for efficient near-infrared photothermal cancer therapy. Small. 2014; 10: 3139-44.

Cite this article as: He C, Wang S, Yu Y, Shen H, Zhao Y, Gao H, et al. Advances in biodegradable nanomaterials for photothermal therapy of cancer. Cancer Biol Med. 2016; 13: 299-312. doi: 10.20892/j.issn.2095-3941.2016.0052